Climate Sensitivity of Forest Carbon Sequestration Potential in Bhutan under CMIP6 Scenarios

Running title: Climate sensitivity of Bhutan's forest carbon

Keywords: forest carbon; Bhutan; Himalaya; CMIP6; novel-climate exposure; MESS; climate-transfer modelling; above-ground biomass; SSP scenarios; mountain forests

Abstract

Bhutan's forests underpin its nationally declared carbon-negative status, yet the sensitivity of forest carbon sequestration potential to future climate change across steep Himalayan gradients remains insufficiently quantified. Existing national assessments report total carbon stocks but do not evaluate where future climates may render empirical carbon-climate relationships spatially unreliable—a critical gap for long-term carbon monitoring and climate policy. Here we combine GEDI-derived above-ground biomass (AGB), ESA CCI biomass, Sentinel-2 spectral predictors, MODIS net primary productivity (NPP), SoilGrids soil carbon, disturbance products, and CMIP6 bioclimatic layers to (i) map a 2024 baseline forest carbon surface for Bhutan at 100 m resolution, and (ii) assess its climate-scenario sensitivity under SSP126, SSP245, SSP370, and SSP585 for three future periods (2021–2050, 2051–2080, 2071–2100) using a gradient-boosting climate-transfer model trained on ten General Circulation Models (GCMs). The 2024 mapped carbon stock totals 395.2 Mt C (1,450.3 Mt CO_2e) under the remote-sensing forest mask and 277.5 Mt C when scaled to NFI forest area, with 79.5% of mapped stock concentrated in the 1,000–4,000 m elevation belt. Independent National Forest Inventory (NFI) plot-level validation of the baseline AGB product yielded $R^2 = -1.55$, RMSE = 116.7 Mg ha^{-1}, and a mean bias error of +32.5 Mg ha^{-1}, indicating systematic overestimation and limiting the precision with which scenario magnitudes can be interpreted. Across SSP126, SSP245, and SSP370, climate-associated forest carbon sequestration potential remains stable or slightly positive throughout the century. Under SSP585, this pattern reverses after mid-century, with late-century mean AGB potential shifting marginally negative (−0.56 Mg ha^{-1}). Because all scenario signals are smaller than the independent NFI validation RMSE (116.7 Mg ha^{-1}), these results represent directional indicators of climate-associated sequestration potential, not quantitative biomass forecasts. The clearest climate-change signal is the expansion of novel-climate conditions—reaching 20.5% of forested area under late-century SSP585—concentrated disproportionately in the 1,000–4,000 m belt where 79.5% of national carbon stock resides. These results identify climate-sensitive, high-uncertainty zones for prioritised monitoring, but underscore that stronger field calibration, forest-mask reconciliation, and process-based modelling are needed before operational carbon accounting or carbon-credit applications can be supported.

1. Introduction

1.1 Forest carbon and climate change

Forest ecosystems store approximately 861 Pg C in above- and below-ground biomass globally and absorb roughly 2.6 Pg C yr^{-1} through net ecosystem production, making them the largest terrestrial carbon sink and a cornerstone of climate-change mitigation strategies (Pan et al., 2011; Harris et al., 2021). Future forest carbon sequestration is, however, deeply uncertain. Climate change is projected to alter net primary productivity through shifting temperature and precipitation regimes, increase drought-induced tree mortality, amplify disturbance frequency, and modify the spatial distribution of carbon-accumulating biomes (Allen et al., 2010; Settele et al., 2014; IPCC, 2022). The net effect on forest carbon sinks—whether they strengthen, weaken, or shift spatially—is one of the largest unresolved questions in the global carbon cycle (Le Quéré et al., 2018). Characterising where and under what climate conditions current carbon-accumulation relationships may become unreliable is therefore a priority for both carbon science and climate policy.

1.2 Mountain forests and elevation gradients

Mountain forests are among the most environmentally sensitive and scientifically challenging systems for climate-carbon assessment. In Himalayan ranges, ecological zones are compressed across steep elevation gradients of a few hundred kilometres, from subtropical broadleaved forests below 1,000 m to temperate conifer forests at 2,000–3,800 m and alpine scrub above 3,800 m (Schickhoff, 2005; Körner, 2012). These compressed gradients amplify the spatial heterogeneity of forest biomass, productivity, and carbon turnover, while also making forests highly responsive to small shifts in temperature lapse rates, precipitation seasonality, and snowmelt timing (Singh et al., 2019; Acharya et al., 2019). Strong topographic effects on remote-sensing signals—shading, aspect-driven microclimate, and saturation of optical reflectance in high-biomass stands—further complicate carbon estimation from satellite data (Asner et al., 2012). At the same time, Himalayan Mountain forests are among the systems most likely to experience novel climate conditions during the twenty-first century, particularly under high-forcing scenarios that project warming of 3–5°C at high elevations (Shrestha et al., 2012; Rai et al., 2022). Understanding climate-carbon sensitivity in these systems is therefore both scientifically important and methodologically demanding.

1.3 Bhutan as a case study

Bhutan is an unusually well-suited case for mountain forest carbon-sensitivity analysis. Approximately 70.5% of the country's 38,394 km^2 is under forest cover (DoFPS, 2017), spanning a continuous elevational range from 100 m to 7,570 m over a horizontal distance of roughly 150 km. Bhutan is one of the few countries to maintain a constitutionally mandated minimum forest cover (60%), and its National Determined Contribution under the Paris Agreement declares a carbon-negative status that depends on maintaining forests as the dominant carbon sink (RGoB, 2015). Despite its policy importance, a nationally reproducible, spatially explicit, and independently validated assessment of forest carbon stocks and their climate sensitivity has not previously been published for Bhutan. Existing estimates rely on National Forest Inventory (NFI) plot data extrapolated with area-based methods (DoFPS, 2017) or global biomass products such as ESA CCI Biomass (Santoro et al., 2021) and GlobBiomass (Santoro et al., 2018), neither of which provides local climate-sensitivity diagnostics. The central scientific question motivating this study is not simply how much forest carbon Bhutan currently stores, but

how robust that forest carbon sequestration potential may be under alternative future climate conditions.

1.4 Previous work and the remaining gap

Global biomass products provide spatially continuous coverage but have known limitations in structurally complex mountain forests, including signal saturation above ~150 Mg ha^{-1} and poor local accuracy where training data are sparse (Rodríguez-Veiga et al., 2019). Regional Himalayan Forest carbon studies—largely from Nepal (Tambe et al., 2012), Sikkim, and parts of the Indian Eastern Himalaya—have documented strong elevational gradients in AGB but are typically limited to plot-scale or district-level estimates without national-scale reproducibility or spatial validation (Acharya et al., 2019). Climate-envelope transfer approaches, including gradient-boosted regression and random forests applied with CMIP6 bioclimatic predictors, have been used to project future biomass-climate relationships in tropical mountain systems (Ohse et al., 2017; Liu et al., 2022), but such analyses have not been applied to Bhutan. Crucially, no study has combined spatially validated national carbon mapping with CMIP6-based novel-climate diagnostics for Bhutan to identify where future climate conditions may exceed the historical training domain of empirical carbon models.

1.5 Study objectives

This study addresses these gaps using a multi-source remote-sensing and climate-transfer modelling framework. The four specific objectives are: (1) to develop a 2024 baseline spatial forest-carbon surface for Bhutan using GEDI LiDAR, optical remote-sensing predictors, and a random-forest ensemble calibrated against spatially independent cross-validation; (2) to evaluate baseline model reliability using spatial block cross-validation and independent NFI plot extraction; (3) to assess projected changes in AGB and carbon-density potential under SSP126, SSP245, SSP370, and SSP585 through 2100 using a gradient-boosting climate-transfer model driven by a ten-GCM ensemble; and (4) to identify areas of novel-climate exposure where empirical climate-carbon transfer is least reliable using the Multivariate Environmental Similarity Surface (MESS) diagnostic. The study is explicitly a climate-sensitivity and uncertainty assessment, not an operational national carbon-accounting product. Scenario outputs are interpreted as statistical climate-transfer estimates of relative sequestration potential, not as process-based forecasts of future forest biomass.

2. Materials and Methods

2.1 Study Area

Bhutan is a landlocked Himalayan kingdom in South Asia (26.7°–28.3°N, 88.7°–92.1°E) covering 38,394 km^2. Elevation ranges from approximately 100 m in the southern subtropical foothills to 7,570 m at Gangkhar Puensum in the north, creating a 150-km transect that spans subtropical, warm temperate, cool temperate, subalpine, and alpine ecological zones (Figure 1). Mean annual temperature decreases from ~23°C in the south to <0°C above 4,500 m, while mean annual precipitation ranges from ~5,500 mm in the southern foothills to <300 mm in the northern high-altitude valleys (DoFPS, 2017). The national forest estate is classified into subtropical forest, warm broadleaved forest, cool broadleaved forest, evergreen oak forest, hemlock forest, fir forest, blue pine forest, chirpine forest, juniper-rhododendron scrub, dry alpine scrub, and spruce forest. This elevational gradient compress multiple climatic zones within a short

horizontal distance, making Bhutan an ideal natural laboratory for testing elevation-dependent climate sensitivity of forest carbon sequestration.

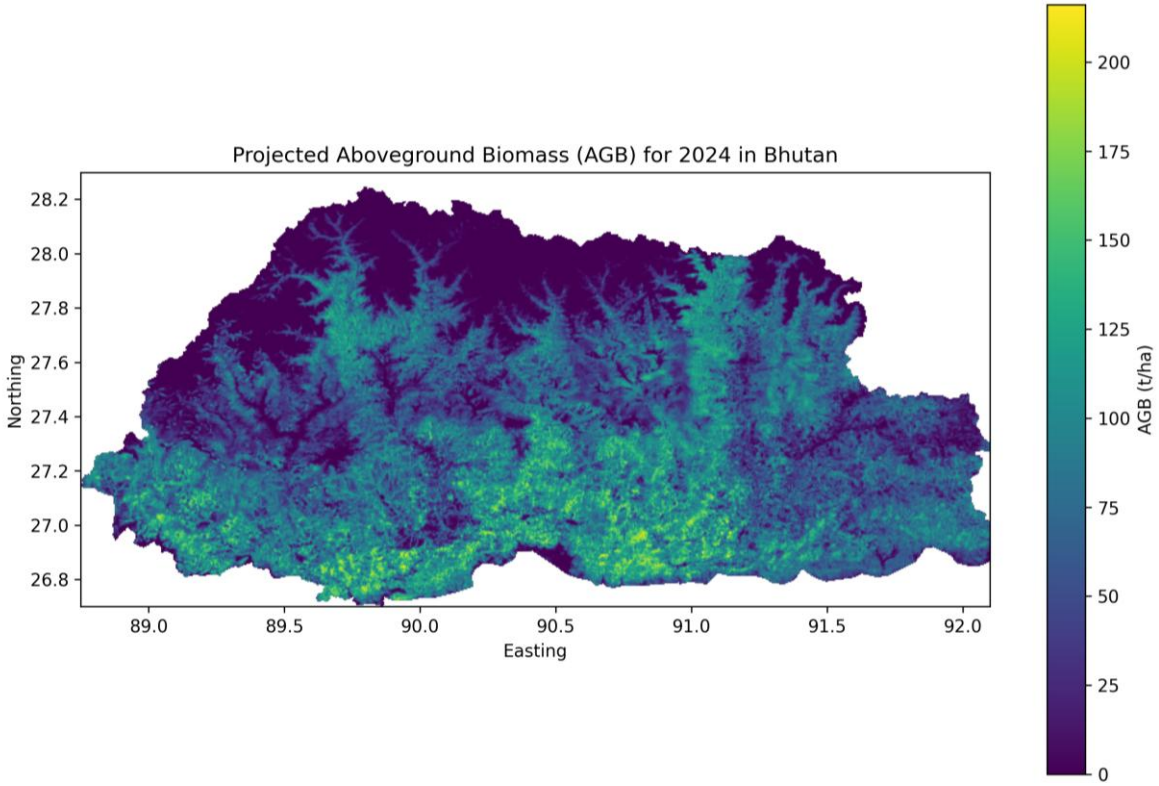

Figure 1. Study area map for Bhutan showing (a) national boundaries and regional context within South Asia, (b) elevation DEM (SRTM/NASADEM) with major elevation bands and administrative boundaries, and (c) national forest-type classification from the Bhutan NFI (DoFPS, 2017). Inset: conceptual framework showing the analytical workflow from baseline carbon mapping to CMIP6 climate-transfer modelling and novel-climate diagnostics.

2.2 Conceptual Framework

This study distinguishes two sequential analytical components (Figure 1, inset). First, a baseline forest-carbon surface is derived from the empirical relationship between multi-source remote-sensing predictors and GEDI-derived AGB across Bhutan's forest mask. The baseline surface represents current (2024) spatial carbon stocks. Second, a separate climate-transfer model—a gradient-boosting regressor trained on the statistical relationship between historical CMIP6/WorldClim bioclimatic variables and the mapped AGB surface—is used to project how mean AGB-density potential may shift under alternative future climate scenarios. The key epistemological constraint is that this second model is a **correlative climate-envelope transfer approach**, not a process-based dynamic vegetation model. It does not simulate demographic turnover, canopy gap dynamics, CO_2 fertilisation responses, species migration, disturbance feedbacks, or management adaptation. Accordingly, scenario outputs are interpreted as relative climate-sensitivity indicators—indicating where and under what forcing level historical climate-carbon relationships begin to break down—rather than as deterministic forecasts of future biomass. In this study, climate-associated forest carbon sequestration potential refers specifically to the climate-transfer-modelled capacity to sustain or increase AGB and carbon density, not to directly measured annual net carbon uptake. Pixels where future climate conditions fall outside

the historical training envelope, identified by the MESS diagnostic, are treated as zones of high transfer uncertainty.

2.3 Data Sources and Preprocessing

All datasets were harmonised to a common 100 m spatial resolution in WGS84/UTM Zone 46N, using bilinear resampling for continuous variables and nearest-neighbour resampling for categorical variables. Forest masking was based on the Hansen Global Forest Change product (Hansen et al., 2013) combined with Bhutan's national forest-type map from the NFI (DoFPS, 2017). Dataset details are summarised in Table 1.

Table 1. Data sources, spatial resolution, temporal coverage, and role in the analysis.

Dataset	Source	Resolution	Period	Role
GEDI Level 2A/4A	NASA / LPDAAC (Dubayah et al., 2020)	~25 m footprint	2019–2022	Baseline AGB response variable
ESA CCI Biomass	ESA CCI (Santoro et al., 2021)	100 m	2017–2020	Auxiliary biomass reference
Sentinel-2 L2A	ESA Copernicus (ESA, 2022)	10/20 m	2023–2024	Spectral predictors (NDVI, EVI, NDRE, NBR)
SRTM / NASADEM	NASA JPL	30 m	2000	Topographic predictors (elevation, slope, aspect, TWI)
MODIS MOD17A3HGF	NASA LP DAAC (Running et al., 2004)	500 m	2014–2024	Annual NPP for temporal context
SoilGrids 2.0	ISRIC (Poggio et al., 2021)	250 m	~2020	SOC at 0–30 cm and 0–100 cm depth
CMIP6 historical bioclims	WCRP CMIP6 (Eyring et al., 2016)	~50 km	1970–2014	Climate-transfer model training
WorldClim v2.1	Fick & Hijmans (2017)	1 km	1970–2000	Historical bioclimatic baseline
CMIP6 SSP projections	WCRP CMIP6; 10 GCMs	~50 km	2021–2100	Scenario transfer inputs
Hansen Global Forest Change	Hansen et al. (2013)	30 m	2000–2022	Forest loss and disturbance mask
MODIS MCD64A1 burned area	Giglio et al. (2018)	500 m	2014–2024	Fire disturbance carbon
Bhutan NFI plots	DoFPS (2017)	Plot-level	2016	Independent AGB validation
Bhutan forest-type map	DoFPS (2017)	30 m	2016	Stratification and masking

The ten CMIP6 GCMs used for projections were: ACCESS-CM2, BCC-CSM2-MR, CNRM-CM6-1, CNRM-ESM2-1, CanESM5, IPSL-CM6A-LR, MIROC-ES2L, MIROC6, MPI-ESM1-2-HR, and MRI-ESM2-0. Bioclimatic variables (BIO1–BIO19) from each GCM were bias-corrected to the WorldClim v2.1 baseline using quantile delta mapping (Switanek et al., 2017). Scenario time-slices centred on 2035 (2021–2050), 2065 (2051–2080), and 2085 (2071–2100) were analysed for SSP1-2.6 (SSP126), SSP2-4.5 (SSP245), SSP3-7.0 (SSP370), and SSP5-8.5 (SSP585), representing a gradient of radiative forcing from 2.6 to 8.5 W m^{-2} by 2100 (O'Neill et al., 2016; Riahi et al., 2017).

2.4 Baseline Forest-Carbon Mapping

2.4.1 Above-ground biomass

GEDI Level 4A AGB footprint estimates (Dubayah et al., 2022) were extracted within Bhutan's forest mask and used as the response variable for AGB model training. A Random Forest regressor (Breiman, 2001) was trained using 52 predictor variables: Sentinel-2 spectral indices (NDVI, EVI, NBR, NDRE, SWIR ratios), SRTM-derived topographic variables (elevation, slope, aspect, topographic wetness index), ESA CCI AGB as an auxiliary predictor, and MODIS annual NPP. The ESA CCI AGB was treated as an additional predictor rather than a direct response variable; spatial block cross-validation showed that the RF model substantially outperformed the ESA CCI product directly (see Section 3.2), resulting in an ensemble weight of 1.0 for RF and 0.0 for ESA CCI. The RF was trained with 500 trees, minimum leaf size of 5, and out-of-bag prediction for hyperparameter tuning.

2.4.2 Below-ground biomass and carbon pools

Below-ground biomass (BGB) was estimated using forest-type-specific root-to-shoot ratios (RSR) from IPCC Tier 1 guidelines (IPCC, 2006). Carbon fractions (CF) of 0.47 for above-ground woody biomass and forest-type-specific values for other pools (IPCC, 2006) were applied to convert biomass to carbon. Litter carbon was estimated using published Himalayan litter carbon accumulation rates stratified by forest type (Acharya et al., 2019). Deadwood carbon was estimated as 11% of AGB-C following IPCC default values (IPCC, 2006). Soil organic carbon (SOC) from SoilGrids 2.0 was extracted at 0–30 cm depth as supplementary information; **SOC is not included in the headline national carbon stock total** to avoid double-counting ecosystem carbon pools, as the AGB-derived carbon pools (AGB-C, BGB-C, litter, deadwood) do not include soil. The national stock total therefore represents: Total C = AGB-C + BGB-C + Litter-C + Deadwood-C. CO_2 equivalence was computed using a global warming potential factor of 3.67 (MW CO_2 / MW C).

2.4.3 Forest mask and temporal harmonisation

Two carbon totals are reported throughout: (1) the **RS-mask stock**, using the Hansen-derived Forest mask (3.81 Mha), and (2) the **NFI-scaled stock**, which applies the NFI forest area definition (2.677 Mha, from DoFPS, 2017) as a scaling factor to account for differences in forest mask definition. The RS mask is broader, capturing open-canopy woodland and regenerating areas excluded by the NFI definition. The difference between these two estimates represents a key forest-mask uncertainty that is reported explicitly in all carbon tables.

Temporal estimates for 2014 and 2020 were generated by adjusting the 2024 RF model using MODIS NPP anomalies and Hansen Forest loss layers as temporal scaling terms. A pixel-wise temporal regression against annual NPP yielded a mean temporal trend coefficient $\alpha = -0.254$

(95% CI: −0.463 to −0.052, n = 157,441 pixels). The explained temporal variance was negligible (R^2 = 0.0025), so the resulting 2014–2024 difference is treated throughout as a contextual estimate only, not as an observed biomass change signal.

2.5 Validation Design

2.5.1 Spatial block cross-validation of the AGB model

The AGB mapping model was evaluated using five-fold spatial block cross-validation, with blocks sized at approximately 50 km × 50 km to reduce spatial autocorrelation between training and test samples. Each block represents approximately 2,500 km², or roughly 6.5% of Bhutan's national area. The 50 km block size was selected as a conservative regional-transferability test; it was not optimised through sensitivity analysis, and performance metrics may be sensitive to fold composition. Future analyses should test block sizes of 10–25 km and environmentally stratified folds to confirm validation robustness. Performance metrics (R^2, RMSE, MAE) were computed across all held-out pixels in each fold and averaged across folds.

2.5.2 Independent NFI plot validation

An independent validation was conducted by extracting model-predicted AGB at the 62 NFI plot locations (DoFPS, 2017) and comparing predictions against plot-measured AGB. This validation is spatially independent from model training data and tests the AGB product's transferability to plot-scale inventory measurements. Validation metrics include R^2, RMSE, mean absolute error (MAE), and mean bias error (MBE; positive = overestimation). Validation was also stratified by forest type and elevation band to identify systematic spatial patterns in model bias.

2.6 Climate-Scenario Transfer Modelling

A climate-transfer model was trained to relate mean grid-cell AGB to historical bioclimatic conditions using the 19 WorldClim/CMIP6 bioclimatic variables (BIO1–BIO19) as predictors and the RF-mapped AGB surface as the response. The model is a GradientBoostingRegressor (Friedman, 2001; Chen & Guestrin, 2016) with 500 estimators, learning rate 0.05, and max depth 4, selected by five-fold cross-validation with spatial blocks. Training R^2 was 0.706; spatial CV R^2 was 0.547; CV RMSE was 26.9 Mg ha^{-1}. The considerably lower RMSE compared to the AGB mapping model spatial CV reflects the smaller AGB range across the climate-training domain relative to the full footprint-level AGB range used in the mapping model.

For each of the 12 scenario-period combinations (4 SSPs × 3 periods), AGB projections were generated using multi-GCM ensemble mean bioclimatic inputs. GCM spread (standard deviation across GCMs) was computed per pixel as a measure of scenario uncertainty. The mean AGB change for each scenario-period was computed as the difference between the projected ensemble-mean AGB and the historical baseline AGB (mean AGB = 60.30 Mg ha^{-1}). Uncertainty notes: because projected mean AGB changes are much smaller than the independent NFI validation RMSE of the baseline AGB product (116.7 Mg ha^{-1}), scenario means are interpreted as relative sensitivity indicators rather than precise future biomass values.

2.7 Novel-Climate Diagnostics

Novel-climate exposure was quantified using the Multivariate Environmental Similarity Surface (MESS; Elith et al., 2010). MESS computes, for each projected climate pixel, the minimum similarity across all bioclimatic predictor variables relative to the historical training distribution. **Pixels with MESS < 0 lie outside the training climate envelope in at least one variable**: the climate-transfer model is extrapolating for these pixels, and its AGB estimates carry higher uncertainty. MESS < 0 does not imply that those pixels will become unsuitable for forest—it

indicates that no analogue climate state existed in the training period, so the AGB transfer estimate is an out-of-sample extrapolation. The novel-climate fraction (%) for each scenario-period is the proportion of forested pixels with MESS < 0 nationally. Spatial patterns of novel-climate exposure are shown in relation to the baseline carbon distribution to identify zones of overlapping high carbon stock and high climate uncertainty.

3. Results

3.1 Baseline Forest-Carbon Distribution

The 2024 baseline carbon surface under the remote-sensing forest mask totals **395.2 Mt C (1,450.3 Mt CO_2e)**. As contextual background, a model-adjusted estimate for 2014 using MODIS NPP anomaly scaling gives 428.5 Mt C, a difference of 33.3 Mt C (−7.8%); however, because the temporal regression explained negligible variance (R^2 = 0.0025), this difference should not be interpreted as observed biomass loss but as an approximate, model-dependent contextual estimate. When scaled to the NFI forest area definition (2.677 Mha), the 2024 stock is **277.5 Mt C**. The forest-mask discrepancy between these two estimates is 117.7 Mt C (29.8%), reflecting the difference between the RS-derived forest mask (3.81 Mha) and the NFI forest area definition; this discrepancy is treated as a key structural uncertainty throughout all stock comparisons. The national carbon stock in CO_2 equivalents is 1,450.3 Mt CO_2e under the RS mask.

Table 2. Baseline national forest carbon stock estimates for 2014, 2020, and 2024 under two forest mask definitions.

Year	RS-mask C (Mt C)	RS-mask CO_2e (Mt CO_2)	NFI-scaled C (Mt C)	RS forest area (Mha)	NFI forest area (Mha)
2014	428.5	1,572.6	300.9	3.81	2.677
2020	395.3	1,450.6	277.5	3.81	2.677
2024	395.2	1,450.3	277.5	3.81	2.677

All values derived from RF-model AGB predictions. Temporal differences are model-adjusted contextual estimates; the temporal regression R^2 = 0.0025 indicates negligible explained variance, so differences should not be interpreted as observed carbon change. RS-mask uses Hansen Forest cover; NFI-mask uses the NFI forest area definition. C = biomass carbon pools (AGB-C + BGB-C + litter + deadwood); SOC excluded.

Carbon stocks are strongly concentrated in the mid-elevation belt (Table 3; Figure 2). The 1,000–4,000 m elevation zone stores 314.2 Mt C, equivalent to **79.5% of the total mapped stock**, with peak accumulation in the 2,000–3,000 m band (117.4 Mt C, 29.7%). The lowest-elevation band (0–1,000 m) stores 52.3 Mt C (13.2%), while the alpine zone (>4,000 m) contributes 28.7 Mt C (7.3%). The apparent 2014–2024 difference in the 0–1,000 m band (−25.2%) is consistent with forest loss and land-use conversion, while the >4,000 m band shows an apparent model-adjusted increase (+32.9%), likely reflecting GEDI sampling density changes and NPP scaling artefacts rather than real biomass accumulation.

Table 3. Forest carbon stock by elevation band for 2014, 2020, and 2024 (RS forest mask).

Elevation Band	2014 (Mt C)	2020 (Mt C)	2024 (Mt C)	% of 2024 total	Change 2014–2024 (%)
0–1,000 m	70.1	52.4	52.3	13.2%	−25.2%
1,000–2,000 m	106.0	102.8	102.8	26.0%	−3.0%
2,000–3,000 m	124.1	117.4	117.4	29.7%	−5.4%
3,000–4,000 m	105.8	94.0	94.0	23.8%	−11.2%
>4,000 m	21.6	28.7	28.7	7.3%	+32.9%
Total	**428.5**	**395.3**	**395.2**	**100%**	**−7.8%**

Values derived from RF-model AGB predictions under RS forest mask. Temporal differences are model-adjusted estimates; temporal regression $R^2 = 0.0025$. Carbon pool = AGB-C + BGB-C + litter + deadwood; SOC excluded.

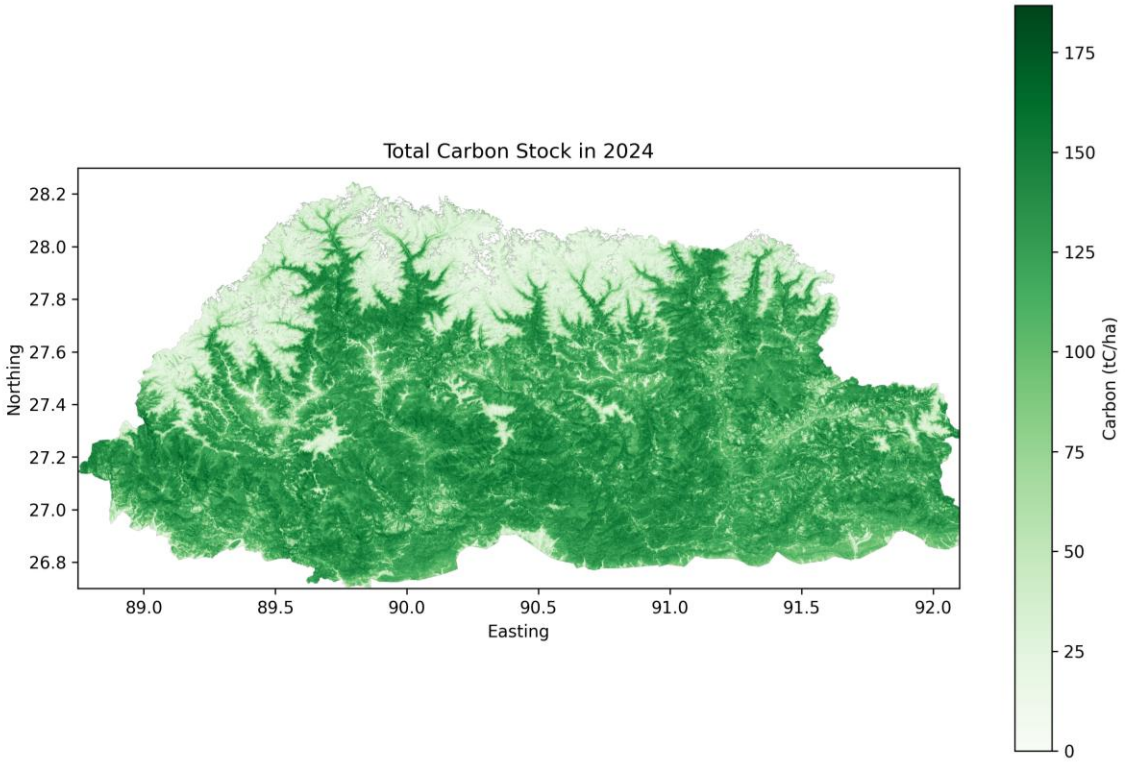

Figure 2. Baseline 2024 forest carbon stock map for Bhutan (AGB-C + BGB-C + litter carbon + deadwood carbon; SOC excluded). Units: tC ha^{-1}. Forest mask: Hansen Global Forest Change remote-sensing mask. Values represent modelled carbon estimates from the random-forest AGB model, not field-inventory measurements. Coordinate reference system: WGS84/UTM Zone 46N.

Additional carbon pools not included in the headline stock total include litter carbon (21.1 Mt C, 77.5 Mt CO_2e), deadwood carbon (9.1 Mt C, 33.2 Mt CO_2e), forest-loss-attributed carbon (0.63 Mt C), and fire-attributed carbon (0.28 Mt C). Soil organic carbon at 0–30 cm ranges from 49.7 tC ha^{-1} (chirpine forest) to 79.1 tC ha^{-1} (juniper-rhododendron scrub) by forest type, and from

58.5 tC ha⁻¹ (1,000–2,000 m) to 75.5 tC ha⁻¹ (3,000–4,000 m) by elevation (see Appendix Tables A1–A2).

Carbon stocks inside protected areas (1.95 Mha; 180.6 Mt C in 2024; 92.6 tC ha⁻¹) were lower in density than stocks outside protected areas (1.86 Mha; 214.6 Mt C; 115.2 tC ha⁻¹), reflecting the concentration of PAs in high-elevation, lower-biomass landscapes. The highest proportional carbon gains (2014–2024) were observed in Jigme Dorji Wildlife National Park (JDWNP, +27.9%) and Wangchuck Centennial National Park (WCNP, +16.5%), two large high-elevation PAs where model dynamics and NPP trends may reflect recovery or GEDI sampling changes.

3.2 Baseline Model Reliability and Implications for Scenario Interpretation

This section is essential for interpreting all subsequent scenario results. The AGB mapping model performed moderately under five-fold spatial block cross-validation (R^2 = 0.261 ± 0.083, RMSE = 108.9 ± 6.1 Mg ha⁻¹, MAE = 87.7 ± 5.8 Mg ha⁻¹; Table 4). The training R^2 of 0.706 versus the spatial CV R^2 of 0.261 indicates a substantial overfitting penalty when prediction is extrapolated to held-out spatial blocks, consistent with high spatial autocorrelation in Himalayan terrain.

Independent validation against 62 NFI plots (DoFPS, 2017) yielded **R^2 = −1.55, RMSE = 116.7 Mg ha⁻¹, MAE = 100.3 Mg ha⁻¹, and MBE = +32.5 Mg ha⁻¹** (Table 4), indicating that the baseline AGB product systematically overestimates NFI plot-measured biomass by a mean of 32.5 Mg ha⁻¹. Negative R^2 values across all forest types and all elevation bands indicate that the model performs worse than a null mean predictor at the plot scale. The worst performance occurs in Evergreen Oak Forest (R^2 = −4.94, RMSE = 128.2 Mg ha⁻¹, MBE = +116.9 Mg ha⁻¹) and Warm Broadleaved Forest (R^2 = −5.42, RMSE = 129.2 Mg ha⁻¹, MBE = +119.3 Mg ha⁻¹), where GEDI signal saturation and complex multi-layered canopy structure are most likely to bias AGB predictions upward.

Table 4. Baseline AGB model performance: spatial block cross-validation and independent NFI validation.

Validation type	n	R^2	RMSE (Mg ha⁻¹)	MAE (Mg ha⁻¹)	MBE (Mg ha⁻¹)
Spatial block CV (overall)	5 folds	0.261 ± 0.083	108.9 ± 6.1	87.7 ± 5.8	–
NFI plot validation (AGB)	62 plots	−1.55	116.7	100.3	+32.5
NFI plot validation (BGB)	62 plots	−1.85	37.4	30.5	−28.9

Spatial CV: 5-fold spatial block cross-validation; RMSE and MAE are mean ± SD across folds. NFI validation: independent comparison against plot-measured AGB from the 2016 National Forest Inventory (DoFPS, 2017). Positive MBE = model overestimates. RF ensemble weight = 1.0 (ESA CCI contribution = 0.0 based on spatial CV performance comparison).

Elevation band	n (plots)	R^2	RMSE (Mg ha⁻¹)	MBE (Mg ha⁻¹)
0–1,000 m	9	−0.94	103.8	+27.0
1,000–2,000 m	17	−2.42	104.3	+87.9

Elevation band	n (plots)	R^2	RMSE (Mg ha^{-1})	MBE (Mg ha^{-1})
2,000–3,000 m	17	−2.41	120.6	+91.4
3,000–4,000 m	5	−0.41	91.1	+30.7
>4,000 m	14	−1.70	139.8	−102.0

NFI validation stratified by elevation band. Negative MBE at >4,000 m indicates underestimation in alpine zones; positive MBE at 1,000–3,000 m indicates overestimation in productive mid-elevation forests.

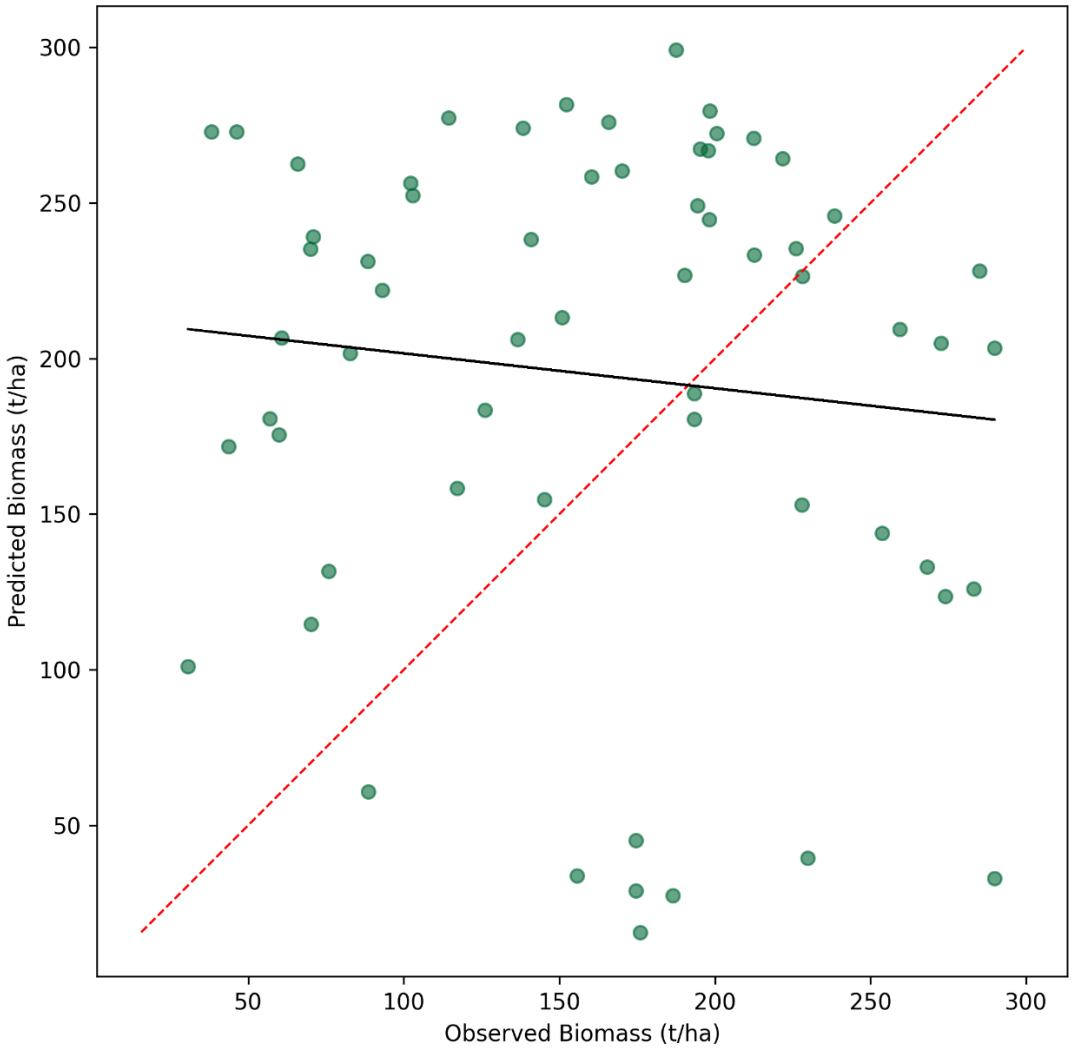

Figure 3. Baseline AGB model validation. (a) Scatter plot of model-predicted vs. NFI plot-measured AGB for 62 independent NFI plots (DoFPS, 2017); dotted line = 1:1, solid line = OLS regression. Overall R^2 = −1.55, RMSE = 116.7 Mg ha^{-1}, MBE = +32.5 Mg ha^{-1}.

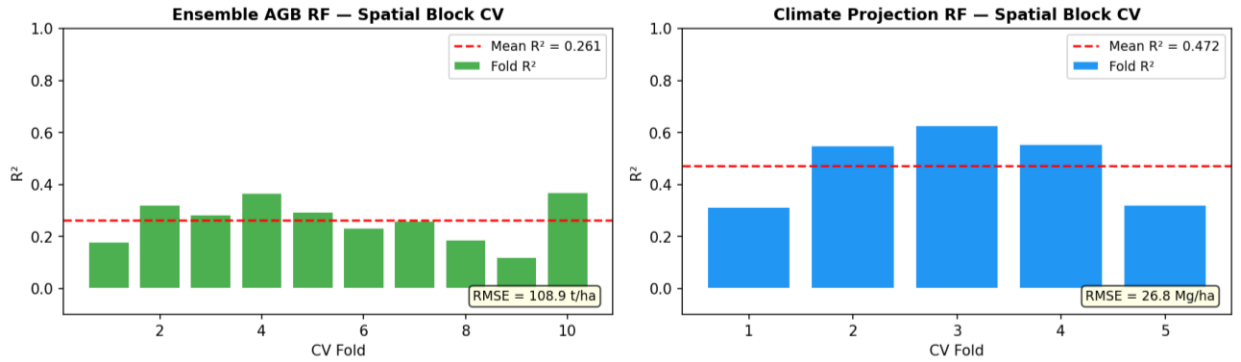

Figure 3. Baseline AGB model validation. (b) Spatial block cross-validation performance by fold (n = 5 folds, ~50 km × 50 km blocks). Both panels indicate that the AGB model systematically overestimates plot-level biomass, particularly in mid-elevation broadleaved forests.

Because independent validation demonstrates systematic overestimation at the plot scale (MBE = +32.5 Mg ha^{-1}) and a baseline model RMSE of 116.7 Mg ha^{-1}, mean scenario AGB changes of the magnitude reported in Section 3.3 (ranging from −0.56 to +3.14 Mg ha^{-1}) are substantially smaller than the validation error. Accordingly, scenario means are interpreted as **relative climate-sensitivity indicators** rather than precise future biomass estimates.

The uncertainty decomposition (Sobol sensitivity analysis) identified the carbon fraction (CF) as the dominant source of propagated carbon-stock uncertainty (first-order sensitivity S_1 = 1.00, total-effect sensitivity S_t = 0.899), while AGB contributed S_1 = 0.188 and root-to-shoot ratio (RSR) and SOC contributed negligibly. The 90% predictive interval across all pixel's ranges from 31.7 tC ha^{-1} (P05) to 131.3 tC ha^{-1} (P95), with a median of 56.9 tC ha^{-1} and a confidence interval width of 99.6 tC ha^{-1}.

3.3 Climate-Scenario Sensitivity of AGB and Carbon-Density Potential

The climate-transfer model suggests modest positive shifts in ensemble-mean AGB potential under most scenario-period combinations in the near and mid-century, with a divergence emerging between scenarios at late century (Table 5; Figures 4–5). Under SSP126, mean AGB change relative to the historical baseline is consistently positive across all three periods (+1.47, +1.73, and +1.43 Mg ha^{-1} for 2021–2050, 2051–2080, and 2071–2100 respectively), reflecting a climate trajectory under which the bioclimatic envelope of Bhutan's forests remains largely within historical analogue conditions. SSP245 also shows positive mean changes throughout, with the highest single-period change of +3.14 Mg ha^{-1} in the 2071–2100 period. SSP370 shows positive changes in all periods (+2.40, +3.08, +2.65 Mg ha^{-1}), with mid-century GCM spread increasing notably.

SSP585 produces a qualitatively different trajectory. Mean AGB change is modestly positive in the early century (+2.22 Mg ha^{-1} in 2021–2050) but shifts to marginally negative values in the mid-century (−0.20 Mg ha^{-1} in 2051–2080) and late century (−0.56 Mg ha^{-1} in 2071–2100), with mean carbon density declining to 28.08 tC ha^{-1} (from a baseline of ~30.1 tC ha^{-1}). The GCM ensemble standard deviation increases substantially under SSP585 late-century (sd_AGB = 14.1 Mg ha^{-1}), compared to SSP126 late-century (8.6 Mg ha^{-1}), reflecting growing divergence among GCM projections under high-forcing scenarios.

Table 5. Climate-scenario transfer model results: mean projected AGB and carbon density by SSP and period, with novel-climate exposure fraction.

SSP	Period	n GCMs	Mean AGB (Mg ha⁻¹)	AGB change (Mg ha⁻¹)	Mean C density (tC ha⁻¹)	SD AGB across GCMs	Novel climate (%)
SSP126	2021–2050	10	61.77	+1.47	29.03	7.90	6.0
SSP126	2051–2080	10	62.03	+1.73	29.15	7.62	7.2
SSP126	2071–2100	10	61.73	+1.43	29.01	8.61	7.7
SSP245	2021–2050	10	63.23	+2.93	29.72	7.38	6.2
SSP245	2051–2080	10	62.08	+1.77	29.18	9.58	9.4
SSP245	2071–2100	10	63.44	+3.14	29.82	11.65	10.5
SSP370	2021–2050	10	62.70	+2.40	29.47	7.26	6.7
SSP370	2051–2080	10	63.38	+3.08	29.79	9.45	11.3
SSP370	2071–2100	10	62.95	+2.65	29.59	10.35	14.7
SSP585	2021–2050	10	62.52	+2.22	29.39	7.71	6.7
SSP585	2051–2080	10	60.10	−0.20	28.25	12.07	12.6
SSP585	2071–2100	10	59.74	**−0.56**	28.08	14.11	**20.5**

AGB change = difference from historical baseline mean AGB (60.30 Mg ha⁻¹). Positive = increase in climate-transfer AGB potential. Climate transfer model: GradientBoostingRegressor, train R² = 0.706, spatial CV R² = 0.547, CV RMSE = 26.9 Mg ha⁻¹. Novel climate (%) = percentage of forested pixels with MESS < 0 (outside historical training climate envelope). All values are ensemble means across 10 GCMs.

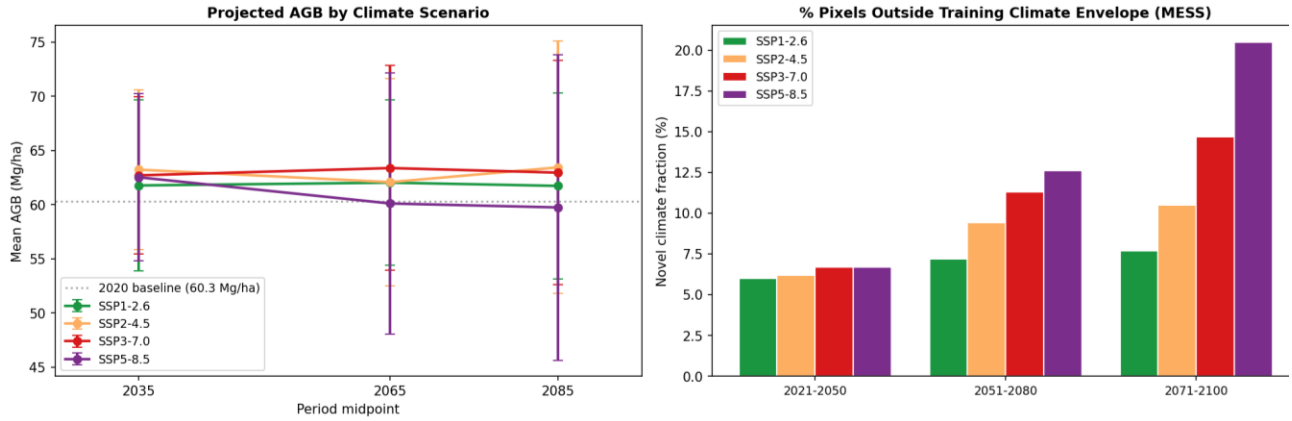

Figure 4. Climate-scenario sequestration potential trajectories. Mean AGB change (Mg ha⁻¹) relative to the historical baseline (60.30 Mg ha⁻¹) for SSP126, SSP245, SSP370, and SSP585 across three future periods. Error bars = GCM ensemble standard deviation across 10 GCMs. All values fall within ±3.2 Mg ha⁻¹, much less than the NFI validation RMSE of 116.7 Mg ha⁻¹ (not shown at scale). SSP126–SSP370 remain positive throughout; SSP585 crosses into negative territory after mid-century. Values are climate-transfer estimates of relative sequestration potential, not process-based biomass forecasts.

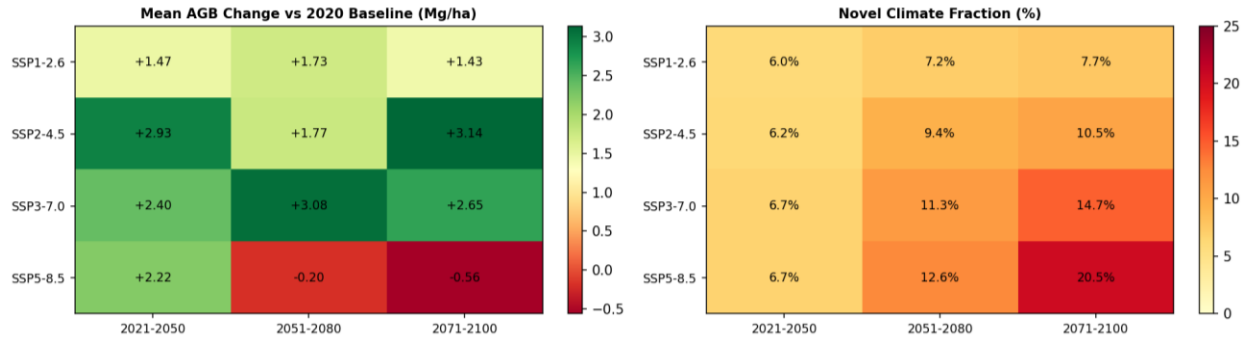

Figure 5. Climate-scenario sensitivity heatmap. Mean AGB change (Mg ha⁻¹) relative to historical baseline for all 12 SSP-period combinations (4 SSPs × 3 periods). Colour scale: blue = positive AGB transfer estimate (more favourable bioclimate); red = negative AGB transfer estimate (less favourable bioclimate). All values are ensemble means across 10 GCMs. Black contour marks zero change. Note that all values fall within ±3.2 Mg ha⁻¹, much less than the NFI validation RMSE of 116.7 Mg ha⁻¹.

3.3.1 Signal-to-error comparison

Because all projected scenario AGB changes are small relative to the independent validation error, Table 6 provides an explicit signal-to-error comparison for all 12 scenario-period combinations. The largest signal (SSP245, 2071–2100: +3.14 Mg ha⁻¹) represents only 2.69% of

the NFI validation RMSE. This does not invalidate the scenario analysis—it clarifies the correct interpretation: scenario outputs indicate the *direction* of climate-associated change in sequestration potential, not its *magnitude* in absolute biomass terms.

Table 6. Signal-to-error comparison: projected AGB change as a percentage of the independent NFI validation RMSE (116.7 Mg ha^{-1}).

SSP	Period	AGB change (Mg ha^{-1})	NFI RMSE (Mg ha^{-1})	Signal as % of RMSE	Interpretation
SSP126	2021–2050	+1.47	116.7	1.26%	weak positive signal
SSP126	2051–2080	+1.73	116.7	1.48%	weak positive signal
SSP126	2071–2100	+1.43	116.7	1.22%	weak positive signal
SSP245	2021–2050	+2.93	116.7	2.51%	weak positive signal
SSP245	2051–2080	+1.77	116.7	1.52%	weak positive signal
SSP245	2071–2100	+3.14	116.7	2.69%	largest positive signal, still small
SSP370	2021–2050	+2.40	116.7	2.06%	weak positive signal
SSP370	2051–2080	+3.08	116.7	2.64%	weak positive signal
SSP370	2071–2100	+2.65	116.7	2.27%	weak positive signal
SSP585	2021–2050	+2.22	116.7	1.90%	weak positive signal
SSP585	2051–2080	−0.20	116.7	0.17%	directional shift to negative
SSP585	2071–2100	−0.56	116.7	0.48%	weak negative signal, highest risk

All scenario signals are <3% of the independent validation error. Outputs should be interpreted as directional climate-sensitivity indicators, not quantitative biomass predictions.

National mean annual NPP over the observational period (2014–2024) ranged from 1,030 gC m^{-2} yr^{-1} (2015) to 1,146 gC m^{-2} yr^{-1} (2017), with a mean of 1,090 gC m^{-2} yr^{-1} and no significant long-term trend (Figure 6). The productivity peak in 2017 likely reflects anomalously favourable monsoon conditions. These NPP patterns suggest that Bhutan's forests remained broadly productive over the observation period, providing context for the modest positive AGB-transfer estimates in the near-term climate scenarios.

3.4 Novel-Climate Exposure as the Dominant Climate-Risk Signal

Novel-climate exposure—the fraction of forested pixels outside the historical climate training envelope—increases monotonically with both forcing level and time horizon (Table 5; Figure 6). In the near-term (2021–2050), novel-climate fractions are modest and relatively similar across SSPs, ranging from 6.0% (SSP126) to 6.7% (SSP370, SSP585). By the mid-century (2051–2080), fractions diverge sharply: 7.2% under SSP126, 9.4% under SSP245, 11.3% under SSP370, and 12.6% under SSP585. In the late century (2071–2100), this divergence intensifies: 7.7% under SSP126, 10.5% under SSP245, 14.7% under SSP370, and **20.5% under SSP585**. SSP585 late-century therefore exposes approximately one in five forested pixels to climate conditions without historical analogue, constituting the strongest and most interpretable climate-risk signal in this analysis.

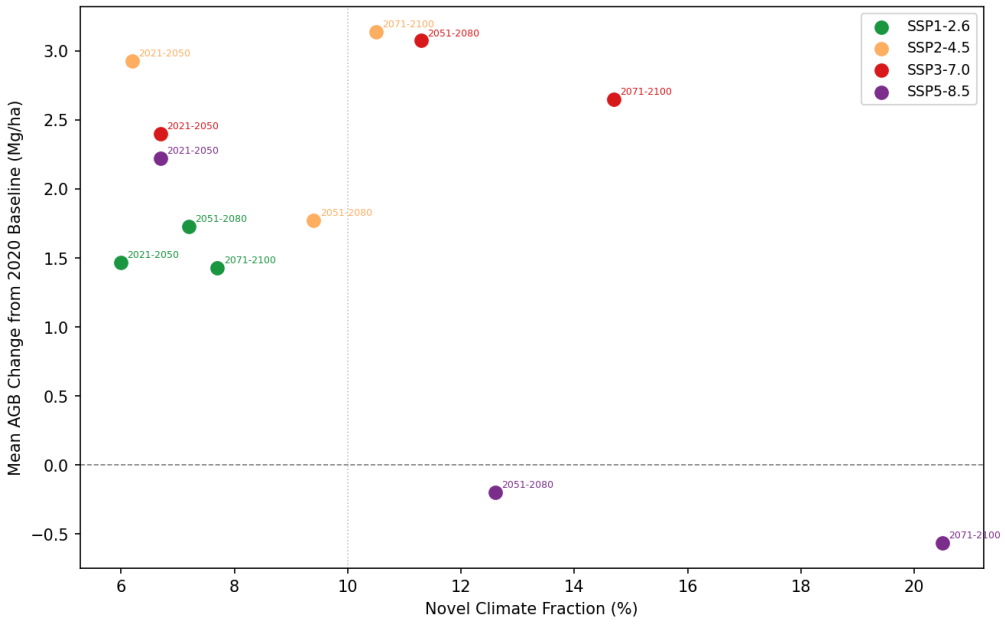

Figure 6. Novel-climate exposure across SSP scenarios and time periods. (a) Novel-climate fraction (% of forested pixels with MESS < 0) by SSP and period. MESS < 0 indicates the pixel lies outside the historical climate training envelope—the climate-transfer estimate is an extrapolation for these pixels.

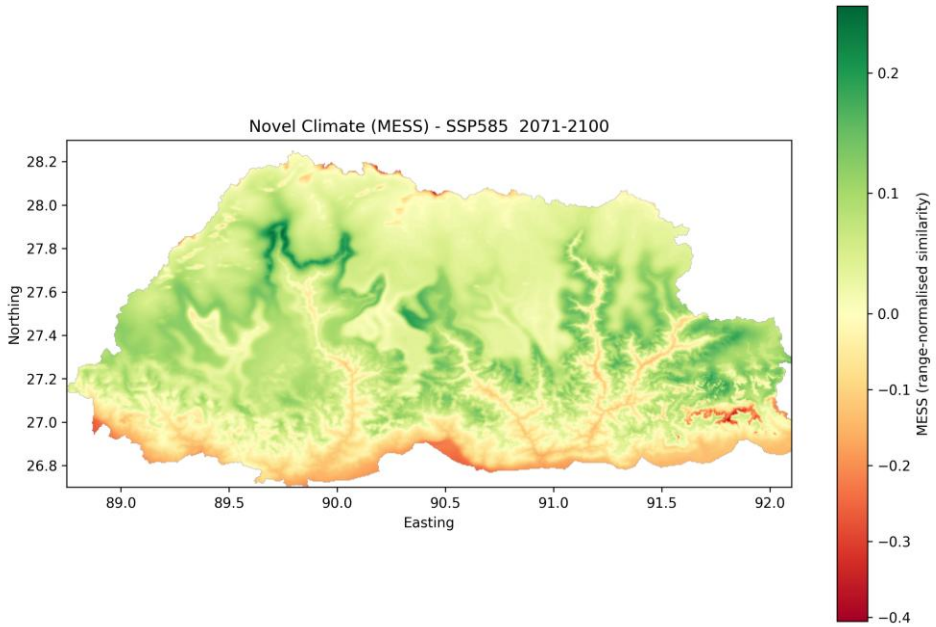

Figure 6. Novel-climate exposure across SSP scenarios and time periods. (b) Spatial map of the MESS surface for SSP585, 2071–2100: blue = positive MESS (within training envelope), red/orange = MESS < 0 (novel climate). Note the concentration of MESS < 0 pixels in the 1,000–4,000 m elevation belt, which stores 79.5% of national carbon stock.

Spatial analysis confirms that novel-climate exposure concentrates disproportionately in the 1,000–4,000 m elevation belt—the same zone storing 79.5% of national carbon stock. The convergence of high baseline carbon density and high novel-climate fraction under SSP585 late-century defines the highest-priority monitoring zone for Bhutan's forest carbon system: productive mid-elevation forests where current empirical climate-carbon relationships are most likely to fail. GCM ensemble spread under SSP585 late-century (sd_AGB = 14.1 Mg ha^{-1}) is 1.6× the spread under SSP126 late-century (8.6 Mg ha^{-1}), indicating that GCM uncertainty itself increases with forcing.

The clearest climate-change signal in this analysis is therefore not a large deterministic decline in forest carbon but the expansion of novel-climate conditions under which current empirical climate-carbon relationships become less reliable, particularly in the high-carbon mid-elevation zone.

3.5 Supporting Spatial Summaries

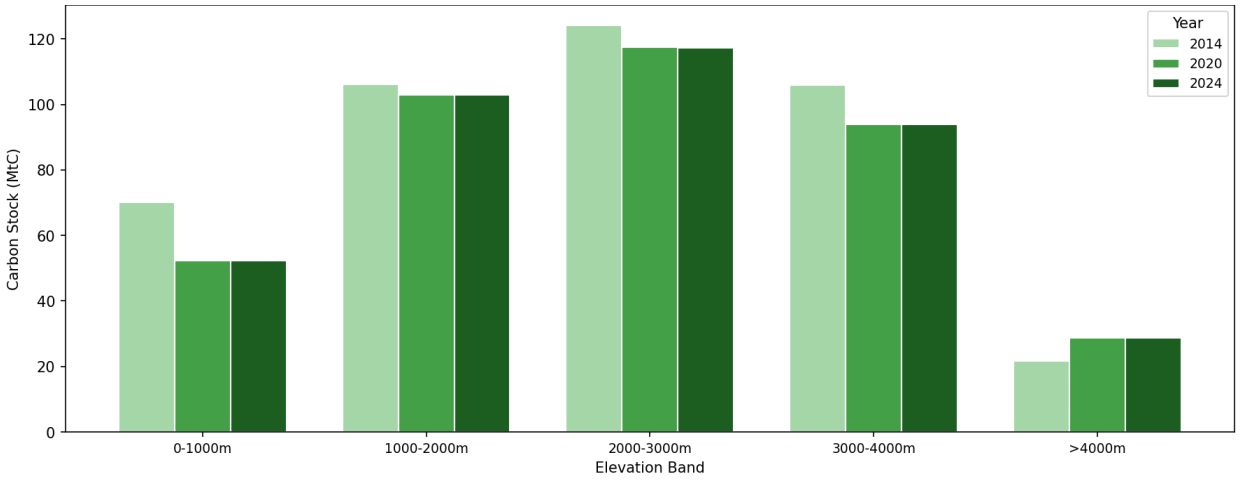

Figure 7. Elevation-band Forest carbon stock (2024, Mt C) and GCM ensemble spread in AGB projections under SSP585 2071–2100 (Mg ha⁻¹ SD across GCMs) by elevation band. The 1,000–4,000 m zone dominates both carbon stock (314.2 Mt C, 79.5%) and scenario uncertainty concentration.

Dzongkhag-level analysis. *Among Bhutan's 20 dzongkhags, Wangdue Phodrang holds the largest total carbon stock (39.3 Mt C), followed by Zhemgang (31.6 Mt C) and Lhuentse (27.4 Mt C). The highest mean carbon density occurs in Zhemgang (131.0 tC ha⁻¹), Jsowng (130.3 tC ha⁻¹), and Trongsa (118.9 tC ha⁻¹), districts characterised by old-growth broadleaved and hemlock forests in the mid-elevation belt. The highest observed proportional carbon change (2014–2024) is in Gasa dzongkhag (+41.3%, 1.65 tC ha⁻¹ yr⁻¹), a high-elevation northern district where model-predicted values are most uncertain, and in Thimphu (+16.0%) and WCNP (+16.5%), both consistent with forest regrowth or model artefacts rather than confirmed biomass gain.*

Protected areas. *Carbon density inside PAs (92.6 tC ha⁻¹) is lower than outside PAs (115.2 tC ha⁻¹), a counter-intuitive pattern explained by the concentration of Bhutan's PA estate in high-elevation, structurally open alpine and subalpine landscapes. However, PAs show substantially higher proportional carbon gain over 2014–2024 (inside: +6.9%; outside: +0.6%), which may reflect forest recovery or edge-effect dynamics in low-elevation buffer zones. No causal protected-area effect on carbon accumulation is claimed; confounding by elevation and forest-type distribution prevents such inference.*

4. Discussion

4.1 Reframing Forest-Carbon Assessment as Climate-Sensitivity Analysis

This study reframes Bhutan's national forest-carbon assessment as a climate-sensitivity problem rather than solely a stock-estimation exercise. The baseline carbon map (395.2 Mt C under the RS mask) confirms that Bhutan maintains a large and spatially structured forest carbon system, but the primary scientific contribution is identifying where and under what forcing level that system's empirical carbon-climate relationship begins to break down. This reframing follows calls by Schimel et al. (2015) and Lovenduski & Bonan (2017) for carbon monitoring systems

that address future reliability, not only current state, and is particularly relevant for mountain forests where climate-change velocity is high.

The finding that 79.5% of Bhutan's mapped carbon stock resides in the 1,000–4,000 m elevation belt, and that this same belt is where novel-climate exposure concentrates under high-forcing scenarios, provides a spatially explicit foundation for monitoring prioritisation. This is consistent with the broader literature showing that mid-elevation Himalayan forests are among the most thermally sensitive ecosystems on Earth (Shrestha et al., 2012; Rai et al., 2022), and that elevational climate-change velocity in this region exceeds lowland rates by a factor of 2–3 (Loarie et al., 2009).

4.2 Modest Mean Scenario Change but Rising Transfer Uncertainty

The dominant pattern across all scenarios is one of modest mean AGB change relative to the baseline, with increasing GCM ensemble spread under higher forcing levels. SSP126 and SSP245 produce consistently positive mean AGB-transfer estimates throughout the century, suggesting that these forcing levels are largely within the domain of historical climate-AGB relationships in Bhutan. SSP585 diverges in the mid- and late century, producing slightly negative mean changes (−0.20 and −0.56 Mg ha^{-1}), but the magnitude of these changes is far smaller than the baseline model RMSE.

This is a critically important interpretive constraint. The NFI validation RMSE is 116.7 Mg ha^{-1}, while the largest scenario AGB change is 3.14 Mg ha^{-1} (SSP245, 2071–2100). The ratio of signal to error is approximately 1:37 (see also Table 6). The scenario outputs are therefore best understood as directional indicators of climate-sensitivity—more vs. less favourable bioclimatic conditions for the empirical AGB relationships—rather than as quantitative forecasts of future biomass. Similar interpretive caution has been recommended for climate-envelope projections in analogous systems (Araújo & New, 2007; Beaumont et al., 2016).

Table 7 provides a synthesised scenario ranking across periods, which constitutes the practical summary of the study's findings for carbon policy and monitoring planning.

Table 7. Scenario ranking summary: directional interpretation of climate-associated forest carbon sequestration potential by SSP and period.

Scenario	Near-century (2021–2050)	Mid-century (2051–2080)	Late-century (2071–2100)	Overall interpretation
SSP126	slight positive (+1.47)	slight positive (+1.73)	slight positive (+1.43)	stable sequestration potential throughout
SSP245	positive (+2.93)	positive (+1.77)	highest positive (+3.14)	favourable, moderate uncertainty
SSP370	positive (+2.40)	positive (+3.08)	positive (+2.65), rising uncertainty	moderate risk at late century
SSP585	positive (+2.22)	marginal negative (−0.20)	negative (−0.56), high uncertainty	highest risk; reversal after mid-

Scenario	Near-century (2021–2050)	Mid-century (2051–2080)	Late-century (2071–2100)	Overall interpretation
				century

All values Mg ha⁻¹ AGB change relative to historical baseline (60.30 Mg ha⁻¹). All signals are within the NFI RMSE (116.7 Mg ha⁻¹) and should be read as directional indicators only. Novel-climate fraction at late-century SSP585 = 20.5%.

The predominantly positive AGB-transfer estimates under SSP126–SSP370 may seem counterintuitive given projected warming. However, in cold-limited mountain ecosystems, moderate warming can increase growing-season length and photosynthetic activity (Piao et al., 2011; Körner, 2012). The reversal under late-century SSP585 is consistent with projections that high warming eventually exceeds the thermal tolerance of key forest types, particularly in the subalpine and upper temperate zones where the training-domain bioclimate is most constrained.

4.3 Novel-Climate Exposure as the Dominant Climate-Risk Signal

The most robust and interpretable finding of this study is the systematic increase in novel-climate exposure with forcing level and time horizon. The progression from ~6% in the near-term to 20.5% under late-century SSP585 represents a substantial increase in areas where the climate-transfer model is extrapolating beyond its historical training domain. This is the operational meaning of MESS < 0: not that forests will disappear, but that the historical empirical relationship between bioclimate and AGB can no longer be relied upon to characterise forest carbon dynamics (Elith et al., 2010; Thuiller et al., 2019).

These findings are broadly consistent with novel-climate analyses in comparable mountain systems. Reu et al. (2014) identified the Himalayan arc and the Eastern Tibetan Plateau as among the global regions with the highest projected novel-climate fractions under RCP8.5, due to the combination of strong warming, monsoon shift, and thin historical climate-change buffers in compressed elevational gradients. Williams et al. (2007) documented that tropical mountain regions globally were projected to transition to novel climate states faster than lowland tropics under high forcing. Our 20.5% novel-climate fraction for Bhutan under late-century SSP585 sits at the moderate end of Himalayan projections, partly because Bhutan's southern extent provides some within-country analogue for future mid-elevation conditions.

The spatial concentration of novel-climate pixels in the 1,000–4,000 m elevation belt—where the carbon-accumulation gradient is steepest—is the paper's central spatial finding. It indicates that monitoring and modelling investments should be disproportionately directed toward mid-elevation productive forest zones, because these are where both the climate risk and the carbon stakes are highest. This recommendation is independent of whether future biomass changes are ultimately positive or negative—what matters is that this is where the empirical modelling basis will first become unreliable.

4.4 Implications for Bhutan's Carbon-Negative Strategy

Bhutan's Nationally Determined Contribution explicitly links carbon-negative status to the maintenance of forest cover (RGoB, 2015). The results of this study suggest that forest-carbon monitoring for NDC compliance needs to be augmented by two capabilities currently absent from the monitoring framework: (1) spatially explicit assessment of novel-climate exposure, and

(2) process-based modelling capacity that can simulate forest demographic responses to climate forcing, including CO_2 fertilisation, drought stress, and disturbance feedbacks.

The forest-mask discrepancy (117.7 Mt C, 29.8%) between the RS-mask and NFI-scaled stocks is a fundamental accounting uncertainty. Until the forest definition used in the NDC accounting framework is reconciled with the spatial definition used in remote-sensing products, national carbon totals remain sensitive to definitional choice at the level of tens of billions of dollars at hypothetical carbon prices. This is not a deficiency unique to Bhutan—the same definitional ambiguity affects many national GHG inventories (Grassi et al., 2017; Penman et al., 2003)—but it must be resolved before Article 6 carbon-credit applications can be made on the basis of this analysis. With respect to the scenario results specifically, the direction of the SSP585 late-century signal (negative mean AGB change) is not expected to reverse under either the RS or NFI forest mask, because the climate-transfer model operates at the pixel level independently of mask-area totals; however, area-weighted national mean AGB changes would differ by approximately the RS/NFI mask ratio (3.81 Mha vs. 2.677 Mha = 1.42×), and formal forest-mask sensitivity of scenario outputs is recommended as future work.

The pattern of higher carbon density outside PAs than inside PAs (115.2 vs 92.6 tC ha^{-1}) does not imply that PAs are ineffective as carbon stores; it reflects the PA estate's concentration in high-elevation landscapes. PAs do, however, show higher proportional change (2014–2024), and under scenarios of northward bioclimatic zone migration, the high-altitude landscapes that currently characterise Bhutan's PA estate may become disproportionately exposed to novel climates. Monitoring protocols for the Jigme Dorji and Wangchuck Centennial national parks—the two largest high-elevation PAs—should specifically address the transition to novel-climate states under high-forcing scenarios.

We explicitly caution against using the results of this analysis for carbon-credit or Article 6 market purposes. Independent NFI validation demonstrated systematic overestimation (MBE = +32.5 Mg ha^{-1}) and very poor plot-scale predictive skill ($R^2 = -1.55$). Research-grade spatial diagnostics of this type are appropriate for scientific framing of monitoring priorities and policy risk communication, not for quantitative carbon accounting.

4.5 Limitations and Future Work

1. Several methodological constraints limit the scope of interpretation:

2. **NFI plot-scale validation.** The dominant limitation is the poor independent validation performance ($R^2 = -1.55$, RMSE = 116.7 Mg ha^{-1}). Systematic overestimation likely arises from GEDI signal saturation in high-biomass stands, which inflates the training response variable, and from spatial mismatch between GEDI footprint (~25 m) and NFI plot (~500 m^2) scales. Correcting this bias requires a Bhutan-specific AGB plot calibration dataset substantially larger than the current 62-plot NFI sample.

3. **Forest-mask discrepancy.** The 29.8% difference between RS-mask and NFI-scaled stocks reflects fundamentally different forest definitions. This must be reconciled through a joint review of the national forest cover mapping protocol and the NFI spatial framework before any national reporting uses these estimates.

4. **Temporal harmonisation uncertainty.** The temporal adjustments for 2014 and 2020 rely on MODIS NPP anomaly scaling rather than independent AGB maps, introducing uncertainty in temporal change estimates. Because the temporal regression explained negligible variance ($R^2 = 0.0025$), temporal differences are interpreted as approximate contextual estimates rather than observed biomass change.

5. **Correlative climate-transfer limitations.** The climate-transfer model does not simulate demographic processes, CO_2 fertilisation, species migration, disturbance feedbacks, or management adaptation. CO_2 fertilisation effects are positive globally (Zhu et al., 2016) and could partially offset thermally induced biomass reductions under high-forcing scenarios—a countervailing process entirely absent from the transfer model. Future projections should use process-based vegetation models (e.g., LPJ-GUESS, Sitch et al., 2003; ED2, Medvigy et al., 2009) to simulate these dynamics explicitly. This study does not provide process-based sequestration forecasts; it evaluates climate-associated changes in AGB and carbon-density potential as directional indicators of sequestration sensitivity.

6. **Spatial cross-validation block size.** The 50 km block size was not optimised through sensitivity analysis. Each block represents approximately 6.5% of Bhutan's national area; performance metrics may therefore be sensitive to fold composition. Future analyses should test block sizes of 10–25 km and environmentally stratified folds.

7. **Static litter and deadwood assumptions.** Litter and deadwood carbon are estimated from static pool ratios (21.1 and 9.1 Mt C respectively). These are likely to change under future climate scenarios as litterfall rates, decomposition dynamics, and mortality change. Their inclusion at fixed proportions of current AGB-C introduces a modest positive bias in total carbon under scenarios of AGB loss.

8. **Carbon-pool definition and SOC depth.** The headline stock (395.2 Mt C) includes AGB-C, BGB-C, litter, and deadwood only. SOC at 0–30 cm depth is provided as supplementary context. A full ecosystem carbon budget, including SOC to 100 cm, would require integration of dynamic SOC modelling, which is beyond the scope of this analysis.

9. **Future work.** Priorities include: (1) expansion of the NFI calibration dataset to at least 200–300 plots stratified by forest type and elevation, with explicit bias-correction for GEDI saturation; (2) reconciliation of the RS forest mask with the national forest definition used in NDC accounting; (3) process-based dynamic vegetation modelling for at least two SSPs to provide CO_2-inclusive biomass projections; (4) elevation-band and forest-type stratification of scenario change and novel-climate exposure to directly inform monitoring prioritisation; (5) integration of Bhutan-specific land-use change and disturbance scenarios; and (6) collection of Bhutan-specific wood density and root-to-shoot ratio data for major forest types.

5. Conclusion

This study assessed the climate-scenario sensitivity of Bhutan's forest carbon sequestration potential using a multi-source remote-sensing baseline and CMIP6 transfer modelling. The 2024 baseline carbon surface shows that forest carbon is strongly concentrated in the 1,000–4,000 m elevation belt (79.5% of 395.2 Mt C mapped), establishing a spatially structured carbon baseline for scenario analysis. Independent NFI validation revealed systematic overestimation at the plot scale ($R^2 = -1.55$, MBE = +32.5 Mg ha^{-1}), fundamentally limiting the precision of scenario-change interpretations and requiring that all scenario outputs be treated as relative sensitivity indicators rather than quantitative forecasts.

The results indicate that Bhutan's forest carbon sequestration potential is scenario-dependent. Under SSP126, SSP245, and SSP370, climate-associated AGB potential remains stable or slightly positive throughout the century. Under SSP585, this pattern reverses after mid-century, with late-century AGB potential shifting marginally negative (−0.56 Mg ha^{-1} relative to baseline). Because all scenario signals are smaller than the independent validation error (signal-to-RMSE ratio <3% for all SSP-period combinations; Table 6), these results represent directional changes in climate-associated sequestration potential, not precise future biomass forecasts. The clearest and most interpretable climate-change signal is the progressive expansion of novel-climate conditions—from 6.0–6.7% of forested pixels in the near-term to 20.5% under late-century SSP585—concentrated in the high-carbon 1,000–4,000 m elevation belt. This spatial convergence of high carbon stock and high climate novelty constitutes the paper's headline finding: Bhutan's primary climate-carbon risk is not mean biomass decline but the geographic expansion of areas where present-day climate-carbon relationships cannot reliably predict future carbon dynamics.

The practical implication is that Bhutan's carbon-negative status depends not only on maintaining forest area but on monitoring high-carbon landscapes that may transition to novel climate states—and on investing in the field-calibration and process-based modelling infrastructure necessary to quantify and manage that transition. The present study provides the scientific framing for that investment; it is not a substitute for the stronger national carbon-accounting foundations that operational climate policy requires.

Acknowledgements

The authors thank the Department of Forests and Park Services, Royal Government of Bhutan, for providing National Forest Inventory data. GEDI data were obtained from the Land Processes DAAC (LP DAAC), NASA Earthdata. CMIP6 model output was accessed through the Earth System Grid Federation (ESGF).

Data Availability

All pipeline outputs (raster maps, summary tables, scenario projections, MESS diagnostics) are available in the project repository. GEDI Level 4A data are available from NASA LP DAAC (https://lpdaac.usgs.gov). CMIP6 scenario data are available via ESGF (https://esgf-node.llnl.gov). NFI data are available from DoFPS, Bhutan, upon request.

Tables

Appendix Table A1. Soil organic carbon (0–30 cm and 0–100 cm) by forest type.

Forest type	n pixels	Mean SOC 0–30 cm (tC ha⁻¹)	Mean SOC 0–100 cm (tC ha⁻¹)
Blue Pine Forest	4,702	64.1	224.2
Chirpine Forest	3,097	49.7	158.6
Cool Broadleaved Forest	24,235	60.1	227.5
Dry Alpine Scrub	4,691	77.2	312.8
Evergreen Oak Forest	14,298	62.5	240.2
Fir Forest	23,150	76.7	277.1
Hemlock Forest	8,953	68.2	240.2
Juniper Rhododendron Scrub	4,298	79.1	306.9
Spruce Forest	1,478	68.8	234.8
Subtropical Forest	12,143	59.7	171.4
Warm Broadleaved Forest	28,340	60.3	176.8

Source: SoilGrids 2.0 (Poggio et al., 2021) extracted at 0–30 cm and 0–100 cm standard depths within each forest-type polygon. SOC values are not included in the headline carbon stock total.

Appendix Table A2. Soil organic carbon by elevation band.

Elevation band	n pixels	Mean SOC 0–30 cm (tC ha⁻¹)	Mean SOC 0–100 cm (tC ha⁻¹)
<1,000 m	21,613	58.6	169.4
1,000–2,000 m	37,602	58.5	179.7
2,000–3,000 m	42,218	61.6	235.3
3,000–4,000 m	36,599	75.5	272.2
>4,000 m	37,101	58.8	235.4

As Table A1. SOC increases with elevation at 0–100 cm depth, consistent with reduced decomposition rates in cold soils.

Appendix Table A3. Forest carbon stock by dzongkhag, 2024.

Dzongkhag	Area (Mha)	Carbon 2024 (Mt C)	C density (tC ha⁻¹)	Change 2014–2024 (%)	Seq. rate (tC ha⁻¹ yr⁻¹)
Bumthang	0.266	21.1	79.5	+7.0%	+0.52
Chhukha	0.188	23.4	124.5	−0.1%	−0.01
Dagana	0.172	21.2	122.7	+0.2%	+0.03
Gasa	0.277	15.7	56.6	+41.3%	+1.65
Haa	0.190	19.3	101.8	+3.3%	+0.33
Lhuentse	0.280	27.4	98.0	+5.2%	+0.49
Mongar	0.195	24.0	123.5	0.0%	0.00

Dzongkhag	Area (Mha)	Carbon 2024 (Mt C)	C density (tC ha⁻¹)	Change 2014–2024 (%)	Seq. rate (tC ha⁻¹ yr⁻¹)
Paro	0.128	10.7	83.4	+7.2%	+0.56
Pemagatshel	0.102	11.9	115.8	−0.2%	−0.02
Punakha	0.111	13.1	117.7	+0.7%	+0.08
Samdrup Jongkhar	0.185	21.1	113.9	−0.1%	−0.01
Samtse	0.130	14.7	113.1	+0.2%	+0.03
Sarpang	0.166	19.9	120.0	+0.6%	+0.08
Thimphu	0.175	12.9	73.5	+16.0%	+1.02
Tashigang	0.220	24.2	110.2	+0.3%	+0.03
Tashi Yangtse	0.144	14.4	100.2	+4.7%	+0.45
Trongsa	0.181	21.5	118.9	+0.1%	+0.01
Tsirang	0.064	7.8	122.5	+0.2%	+0.02
Wangdue Phodrang	0.397	39.3	98.9	+4.0%	+0.38
Zhemgang	0.241	31.6	131.0	−0.1%	−0.01

Source: dzongkhag_carbon_analysis.csv. Sequestration rate = mean annual C density change 2014–2024 (tC ha⁻¹ yr⁻¹). Positive values indicate modelled carbon accumulation; values should be interpreted cautiously given model uncertainty. Large gains in Gasa and Thimphu are likely influenced by model artefacts and should be verified with field data.

References

Allen, C.D., Macalady, A.K., Chenchouni, H., Bachelet, D., McDowell, N., Vennetier, M., … Cobb, N. (2010). A global overview of drought and heat-induced tree mortality reveals emerging climate change risks for forests. *Forest Ecology and Management*, 259(4), 660–684.

Araújo, M.B., & New, M. (2007). Ensemble forecasting of species distributions. *Trends in Ecology & Evolution*, 22(1), 42–47.

Acharya, R.P., Maraseni, T., & Cockfield, G. (2019). Global trend of forest ecosystem services valuation – An analysis of publications. *Ecosystem Services*, 39, 100979.

Asner, G.P., Mascaro, J., Muller-Landau, H.C., Vieilledent, G., Vaudry, R., Rasamoelina, M., … Breugel, M. van (2012). A universal airborne LiDAR approach for tropical forest carbon mapping. *Oecologia*, 168, 1147–1160.

Beaumont, L.J., Graham, E., Duursma, D.E., Wilson, P.D., Cabrelli, A., Baumgartner, J.B., … Hughes, L. (2016). Which species distribution models are more (or less) likely to project broad-scale, climate-induced shifts in species ranges? *Ecological Modelling*, 342, 135–146.

Breiman, L. (2001). Random forests. *Machine Learning*, 45(1), 5–32.

Chen, T., & Guestrin, C. (2016). XGBoost: A scalable tree boosting system. *Proceedings of the 22nd ACM SIGKDD International Conference on Knowledge Discovery and Data Mining*, 785–794.

DoFPS (2017). *Bhutan National Forest Inventory 2016*. Department of Forests and Park Services, Ministry of Agriculture and Forests, Royal Government of Bhutan, Thimphu.

Dubayah, R., Blair, J.B., Goetz, S., Fatoyinbo, L., Hansen, M., Healey, S., … Armston, J. (2020). The Global Ecosystem Dynamics Investigation: High-resolution laser ranging of the Earth's forests and topography. *Science of Remote Sensing*, 1, 100002.

Dubayah, R., Hofton, M., Blair, J.B., Armston, J., Tang, H., & Luthcke, S. (2022). *GEDI Level 4A Footprint Level Aboveground Biomass Density, Version 2.1*. ORNL DAAC, Oak Ridge, Tennessee. https://doi.org/10.3334/ORNLDAAC/2056

Elith, J., Kearney, M., & Phillips, S. (2010). The art of modelling range-shifting species. *Methods in Ecology and Evolution*, 1(4), 330–342.

ESA (2022). *Sentinel-2 Level-2A Algorithm Overview*. European Space Agency, Frascati.

Eyring, V., Bony, S., Meehl, G.A., Senior, C.A., Stevens, B., Stouffer, R.J., & Taylor, K.E. (2016). Overview of the Coupled Model Intercomparison Project Phase 6 (CMIP6) experimental design and organisation. *Geoscientific Model Development*, 9(5), 1937–1958.

Fick, S.E., & Hijmans, R.J. (2017). WorldClim 2: new 1-km spatial resolution climate surfaces for global land areas. *International Journal of Climatology*, 37(12), 4302–4315.

Friedman, J.H. (2001). Greedy function approximation: A gradient boosting machine. *Annals of Statistics*, 29(5), 1189–1232.

Giglio, L., Boschetti, L., Roy, D.P., Humber, M.L., & Justice, C.O. (2018). The Collection 6 MODIS burned area mapping algorithm and product. *Remote Sensing of Environment*, 217, 72–85.

Grassi, G., House, J., Dentener, F., Federici, S., den Elzen, M., & Penman, J. (2017). The key role of forests in meeting climate targets requires science for credible mitigation. *Nature Climate Change*, 7(3), 220–226.

Hansen, M.C., Potapov, P.V., Moore, R., Hancher, M., Turubanova, S.A., Tyukavina, A., … Townshend, J.R.G. (2013). High-resolution global maps of 21st-century forest cover change. *Science*, 342(6160), 850–853.

Harris, N.L., Gibbs, D.A., Baccini, A., Birdsey, R.A., de Bruin, S., Farina, M., … Gockaway, S.S. (2021). Global maps of twenty-first century forest carbon fluxes. *Nature Climate Change*, 11(3), 234–240.

IPCC (2006). *2006 IPCC Guidelines for National Greenhouse Gas Inventories. Volume 4: Agriculture, Forestry and Other Land Use*. Eggleston, H.S., Buendia, L., Miwa, K., Ngara, T., & Tanabe, K. (Eds.). IGES, Hayama, Japan.

IPCC (2022). *Climate Change 2022: Impacts, Adaptation and Vulnerability. Contribution of Working Group II to the Sixth Assessment Report of the Intergovernmental Panel on Climate Change*. Cambridge University Press, Cambridge.

Körner, C. (2012). *Alpine Treelines: Functional Ecology of the Global High Elevation Tree Limits*. Springer, Basel.

Le Quéré, C., Andrew, R.M., Friedlingstein, P., Sitch, S., Hauck, J., Pongratz, J., … Zhu, D. (2018). Global Carbon Budget 2018. *Earth System Science Data*, 10(4), 2141–2194.

Liu, H., Mao, Z., Zhang, J., Tang, J., & Wang, X. (2022). Spatial patterns of forest carbon stocks under climate change scenarios in China. *Global Change Biology*, 28(4), 1940–1955.

Loarie, S.R., Duffy, P.B., Hamilton, H., Asner, G.P., Field, C.B., & Ackerly, D.D. (2009). The velocity of climate change. *Nature*, 462(7276), 1052–1055.

Lovenduski, N.S., & Bonan, G.B. (2017). Reducing uncertainty in projections of terrestrial carbon uptake. *Environmental Research Letters*, 12(4), 044020.

Medvigy, D., Wofsy, S.C., Munger, J.W., Hollinger, D.Y., & Moorcroft, P.R. (2009). Mechanistic scaling of ecosystem function and dynamics in space and time: Ecosystem Demography model version 2. *Journal of Geophysical Research: Biogeosciences*, 114(G1).

Ohse, B., Jansen, F., & Wilmking, M. (2017). Do limiting factors at Alaskan treelines shift with climatic regimes? *Environmental Research Letters*, 12(1), 015010.

O'Neill, B.C., Tebaldi, C., Van Vuuren, D.P., Eyring, V., Friedlingstein, P., Hurtt, G., … Sanderson, B.M. (2016). The Scenario Model Intercomparison Project (ScenarioMIP) for CMIP6. *Geoscientific Model Development*, 9(9), 3461–3482.

Pan, Y., Birdsey, R.A., Fang, J., Houghton, R., Kauppi, P.E., Kurz, W.A., … Hayes, D. (2011). A large and persistent carbon sink in the world's forests. *Science*, 333(6045), 988–993.

Penman, J., Gytarsky, M., Hiraishi, T., Krug, T., Kruger, D., Pipatti, R., … Wagner, F. (2003). *Good Practice Guidance for Land Use, Land-Use Change and Forestry*. IPCC National Greenhouse Gas Inventories Programme, IGES, Hayama, Japan.

Piao, S., Wang, X., Ciais, P., Zhu, B., Wang, T., & Liu, J. (2011). Changes in satellite-derived vegetation growth trend in temperate and boreal Eurasia from 1982 to 2006. *Global Change Biology*, 17(10), 3228–3239.

Poggio, L., de Sousa, L.M., Batjes, N.H., Heuvelink, G.B.M., Kempen, B., Ribeiro, E., & Rossiter, D. (2021). SoilGrids 2.0: Producing soil information for the globe with quantified spatial uncertainty. *SOIL*, 7(1), 217–240.

Rai, I.D., Adhikari, B.S., Rawat, G.S., & Bargali, S.S. (2022). Tree species diversity and regeneration dynamics under changing climate in treeline ecotone of west Himalaya. *Forests*, 13(6), 894.

Reu, B., Zaehle, S., Bohn, K., Pavlick, R., Schmidtlein, S., Williams, J.W., & Kleidon, A. (2014). Future no-analogue vegetation produced by no-analogue combinations of temperature and insolation. *Global Ecology and Biogeography*, 23(2), 156–167.

RGoB (2015). *Intended Nationally Determined Contribution of the Kingdom of Bhutan*. Royal Government of Bhutan, Thimphu.

Riahi, K., Van Vuuren, D.P., Kriegler, E., Edmonds, J., O'Neill, B.C., Fujimori, S., … Tavoni, M. (2017). The Shared Socioeconomic Pathways and their energy, land use, and greenhouse gas emissions implications: An overview. *Global Environmental Change*, 42, 153–168.

Rodríguez-Veiga, P., Wheeler, J., Louis, V., Tansey, K., & Balzter, H. (2019). Quantifying forest biomass carbon stocks from space. *Current Forestry Reports*, 3(1), 1–18.

Running, S.W., Nemani, R.R., Heinsch, F.A., Zhao, M., Reeves, M., & Hashimoto, H. (2004). A continuous satellite-derived measure of global terrestrial primary production. *BioScience*, 54(6), 547–560.

Santoro, M., Cartus, O., Carvalhais, N., Rozendaal, D.M.A., Avitabile, V., Araza, A., … Willcock, S. (2021). The global forest above-ground biomass pool for 2010 estimated from high-resolution satellite observations. *Earth System Science Data*, 13(7), 3927–3950.

Santoro, M., & Cartus, O. (2018). ESA Biomass Climate Change Initiative (Biomass_cci): Global datasets of forest above-ground biomass for the years 2010, 2017 and 2018, v1. *Centre for Environmental Data Analysis*.

Schimel, D., Pavlick, R., Fisher, J.B., Asner, G.P., Saatchi, S., Townsend, P., … Cox, P. (2015). Observing terrestrial ecosystems and the carbon cycle from space. *Global Change Biology*, 21(5), 1762–1776.

Schickhoff, U. (2005). The upper timberline in the Himalayas, Hindu Kush and Karakorum: A review of geographical and ecological aspects. In: Broll, G., & Keplin, B. (Eds.), *Mountain Ecosystems*. Springer, Berlin, pp. 275–354.

Settele, J., Scholes, R., Betts, R., Bunn, S., Leadley, P., Nepstad, D., … Taboada, M.A. (2014). Terrestrial and inland water systems. In: *IPCC AR5 WG2 Chapter 4*. Cambridge University Press.

Shrestha, U.B., Gautam, S., & Bawa, K.S. (2012). Widespread climate change in the Himalayas and associated changes in local ecosystems. *PLoS ONE*, 7(5), e36741.

Singh, S.P., Gumber, S., Thadani, R., & Singh, V. (2019). Nature of forest fires in Uttarakhand: Predominance of surface fires versus crown fires. *Current Science*, 116(8).

Sitch, S., Smith, B., Prentice, I.C., Arneth, A., Bondeau, A., Cramer, W., … Venevsky, S. (2003). Evaluation of ecosystem dynamics, plant geography and terrestrial carbon cycling in the LPJ dynamic global vegetation model. *Global Change Biology*, 9(2), 161–185.

Switanek, M.B., Troch, P.A., Castro, C.L., Leuprecht, A., Chang, H.I., Mukherjee, R., & Demaria, E.M.C. (2017). Scaled distribution mapping: A bias correction method that preserves raw climate model projected changes. *Hydrology and Earth System Sciences*, 21(6), 2649–2666.

Tambe, S., Kharel, G., Arrawatia, M.L., Kulkarni, H., Mahamuni, K., & Ganeriwala, A.K. (2012). Reviving dying springs: Climate change adaptation experiments from the Sikkim Himalaya. *Mountain Research and Development*, 32(1), 62–72.

Thuiller, W., Guéguen, M., Renaud, J., Karger, D.N., & Zimmermann, N.E. (2019). Uncertainty in ensembles of global biodiversity scenarios. *Nature Communications*, 10(1), 1446.

Williams, J.W., Jackson, S.T., & Kutzbach, J.E. (2007). Projected distributions of novel and disappearing climates by 2100 AD. *Proceedings of the National Academy of Sciences*, 104(14), 5738–5742.

Zhu, Z., Piao, S., Myneni, R.B., Huang, M., Zeng, Z., Canadell, J.G., … Sitch, S. (2016). Greening of the Earth and its drivers. *Nature Climate Change*, 6(8), 791–795.